ACS OMEGA

http://pubs.acs.org/journal/acsodf

Article

Remarkable Rate of Water Evaporation through Naked Veins of Natural Tree Leaves

Tukhar Jyoti Konch,[§] Trisha Dutta,[§] Madhurjya Buragohain, and Kalyan Raidongia*

Cite This: *ACS Omega* 2021, 6, 20379–20387

Read Online

ACCESS | Metrics & More | Article Recommendations | Supporting Information

ABSTRACT: In the form of leaves, nature designs the finest photothermal evaporators, and the tremendous evaporation efficiency of leaves is supported by a precisely designed network of veins. Here, we have demonstrated that the vein network of a natural leaf can be extracted through a simple water-assisted digestion process and exploited for low-energy steam generation. The naked leaf veins exhibit a remarkable flux (evaporation rate, 1.5 kg·m^{-2}·h^{-1}) of capillary evaporation under ambient conditions (25 °C and 30% RH), close to the photothermal material-based evaporators reported in the recent literature. Even inside a dark box, naked veins exhibit an evaporation rate up to 4.5 kg·m^{-2}·h^{-1} (at 30% relative humidity (RH) and a wind speed of 22 km·h^{-1}). The mechanistic studies performed with variable atmospheric conditions (temperature, humidity, and wind speed) suggest the evaporation process through the naked veins to be a kinetic-limited process. Naked veins with remarkable evaporation efficiency are found to be suitable for applications like water desalination and streaming potential harvesting. Experiments with the naked veins also unveiled that the biofluidic channels in leaves not only exhibit the characteristics of surface charge-governed ionic transport but also support an exceptional water transport velocity of 1444 μm·s^{-1}.

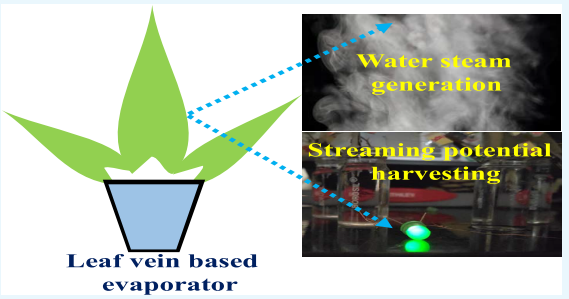

INTRODUCTION

In the past few decades, numerous unforeseen properties and phenomena specific to systems confined in a nanometer-size regime have been uncovered, and many of them have also been exploited for technological applications.[1] One of the recently discovered astonishing nanoscale phenomena is the enormous rate of evaporation from capillary nanochannels.[2−6] In spite of being an ubiquitous natural phenomenon, evaporation through nanoscale capillary channels still lacks thorough understanding and undisputed mechanism.[2] The remarkable evaporation efficiency demonstrated by different nanocapillary systems has been attributed to diverse mechanisms. For example, evaporation fluxes of ultrathin graphene capillaries were observed to be up to two orders of magnitude higher than the one predicted by the classical Hertz−Knudsen (H−K) equation, which was attributed to an extension of the actual evaporation areas.[3] Similarly, in precisely controlled experiments with hybrid two-dimensional nanochannels, Li *et al.* observed that the velocities of water vapor leaving the interface can be larger than the root mean square (RMS) velocities of vapor at the same temperature.[2] This extraordinary observation with individual nanochannels was credited to decreasing thermal resistance between the solid substrate and the liquid/vapor interface, along with an efficient heat and mass transfer process. Similarly, in clear contrast to the typical evaporation behavior, Gimenez *et al.* observed that sessile droplets placed on nonporous surfaces evaporate more rapidly when the salt concentration increases and the temperature decreases. This unexpected evaporation behavior was related to the generation of a steady-state wetted annulus in the droplet periphery.[4]

In spite of being a poorly understood phenomenon, evaporation from nanocapillaries has an enormous impact on our ecological systems. For example, the remarkable capillary evaporation through natural tree leaves is the root of the environmental water cycle.[7] A natural plant leaf transpires a massive amount of water from the soil. Above 95% of the water absorbed by the roots is lost through the openings of stomata via transpiration.[8,9] The rapid evaporation of water through plant leaves is supported by the highly specialized network of xylem.[10−12] The hierarchical and porous veins provide the leaf not only with physical and chemical robustness but also with an ideal platform for the rapid evaporation of water molecules.[13] In this article, we have studied evaporation behavior through the hierarchical structure of the vein network extracted from the fallen leaves and exploited the same for seawater desalination. We observed that even in the absence of photoactive materials, the naked vein network exhibited an evaporation rate on a par with the man-made systems with highly efficient photothermal

Received: May 7, 2021
Accepted: July 12, 2021
Published: July 29, 2021

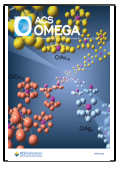

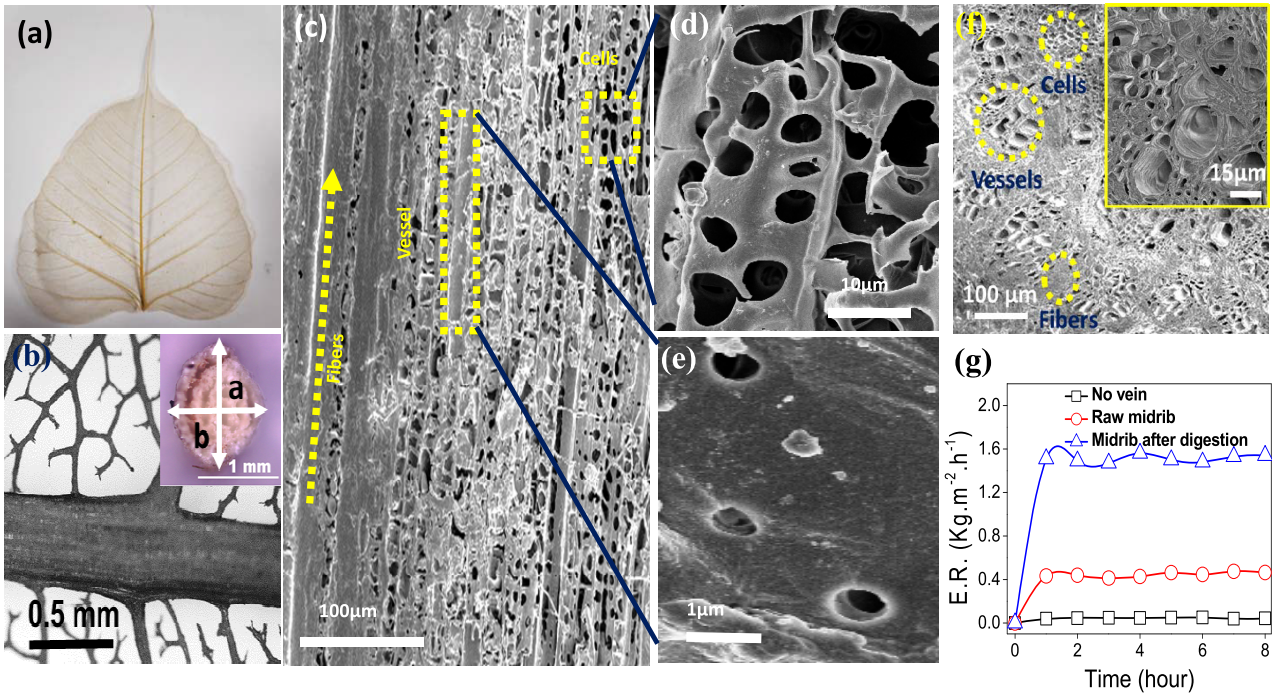

Figure 1. Naked veins of a tree leaf. (a) Digital photo and (b) optical microscopic image of a vein network extracted by removing the digested soft cells of a fallen leaf of *F. religiosa* (Peepal tree). Inset showing the optical microscopic image of the cross section of an isolated midrib vein. (c) FESEM image of the outer surface of an isolated midrib vein along the growth direction showing the different water transportation pathways, *viz.*, vessels, parenchyma cells, and fiber tracheids. FESEM images showing the zoom-in view of (d) parenchyma cells and (e) intervessel pits. (f) Cross-sectional FESEM image of a leaf midrib vein (inset shows a higher-magnification view). (g) The evaporation rate ($E.R._{vein}$) of DI water through a raw midrib vein and isolated midrib vein extracted via the digestion process is compared with that of a similar ampoule without the vein.

materials. A remarkable kinetically controlled evaporation process powered by an extended evaporation area, decreasing thermal resistance between the solid substrate and the liquid/vapor interface, and efficient exchange of heat and mass between water molecules confined inside porous biological channels and atmosphere is accounted for the remarkable performance of the leaf vein-based natural evaporator.

RESULTS AND DISCUSSION

The network of hierarchical channels, precisely designed by nature for efficient transportation of liquids, was extracted from mature and fallen leaf samples collected directly from nature. To begin with, the leaves of *Ficus religiosa* (Peepal tree) were soaked in tap water for around 25 days. During the prolonged soaking period, most of the soft cells of the leaf blade (cuticle, epidermis, and mesophyll) were digested by the microbes, releasing a funky smell. Remarkably, the vein structure of leaf epipodium was not affected by the digestion process. The hierarchical structure of a natural leaf is primarily comprised of high-crystalline cellulose, hemicellulose, and lignin. While lignin possesses an extremely complex structure and dark color, cellulose and hemicellulose are colorless.[14] The digestive process removed most of the soft cells of the leaf blade along with the lignin portion, producing a light-colored system as compared to its natural analogue, shown in Supporting Figure S1a. The FT-IR spectra of a raw leaf vein (Supporting Figure S1b) exhibit intense bands in the regions of 3430 cm^{-1} (O−H stretching vibration), 2900 cm^{-1} (C−H stretching vibration), 1734 cm^{-1} (C═O stretching vibration), 1506 and 1460 cm^{-1} (aromatic C═C stretching vibration), and 1260 cm^{-1} (C−O−C stretching vibration). These bands are related to the hydroxyl groups in celluloses, the carbonyl group of acetyl ester in hemicelluloses and carbonyl aldehyde, and the aromatic skeleton in lignin and guaiacyl ring breathing with C−O stretching, respectively.[14−17] After the digestive process, the intensity of aromatic skeletal bands at 1506 and 1460 cm^{-1} along with the guaiacyl ring breathing with C−O stretching has been significantly reduced, confirming the partial removal of lignin.[17] However, the lignin removal did not seem to perturb the inherent cellulosic skeleton as most of the cellulosic hydroxyl groups are retained. Moreover, the digestive process did not seem to alter the dimension of the leaf veins, suggesting that the original hierarchical alignment of microchannels is well preserved. Instead, the lignin removal creates additional microcapillaries, which can be viewed from the optical microscopic images (Supporting Figure S2).

The digested soft cells were gently removed with a soft brush to isolate the naked vein structure. The veins of a Peepal leaf were chosen due to their mechanical robustness; a typical midrib of a Peepal leaf weighing 50 mg can hold around 400 mg of weight as shown in Supporting Figure S3a. The stress vs strain curve of a delignified midrib vein compared with that of a pristine leaf vein in Supporting Figure S3b indicates that the lignification process made the leaf vein more ductile. Young's moduli of the pristine and delignified midrib veins were calculated to be 30 and 12 MPa, respectively. A digital photo of the extracted vein network is shown in Figure 1a. A thorough examination on multiple optical and electron microscopic images of the vein network (Figure 1b and Supporting Figure S4) with the help of the image processing software ImageJ revealed that about 70% area of the naked vein network is empty or bereft of any channels. The density of the midrib vein was evaluated with the help of BJH analysis to be 1.75 $g{\cdot}cm^{-3}$. Moreover, the leaf vein density, which is defined as the total length of veins per unit area, was evaluated with the help of the

https://doi.org/10.1021/acsomega.1c02398
ACS Omega 2021, 6, 20379−20387

image processing software ImageJ (Supporting Figure S5) and was found to be 2.5 cm^{-1}. The optical microscopic image of the cross section of an isolated midrib vein, shown in the inset of Figure 1b, reveals the presence of large empty channels with diameters extending up to hundreds of micrometers. The optical microscopic investigation also revealed that the typically isolated midrib veins exhibit an oval-like shape. The hierarchical nature of the naked veins can be visualized from the field emission scanning electron microscopic (FESEM) image in Figure 1c. Primarily, natural leaf veins are made of three kinds of cells, fiber tracheids, vessels, and parenchyma cells, as shown in Figure 1c,f. Owing to their large lumen diameter and open-ended wall structure, vessels are the primary conduits for mass transport, whereas the thinner fiber tracheids with closed tapered ends are attributed for the mechanical support.[18,19] Moreover, small pits with an average diameter of ~1 μm are visible on the internal surface of the microchannels (Figure 1e).

To study the evaporation behavior through naked leaf veins, a portion of the midrib (length, 4.7 cm) was isolated from the network by cutting away the secondary veins, as shown in the inset of Figure 1g. The bottom part of the isolated midrib (3.12 cm) was soaked into a glass ampoule containing 15 mL of deionized (DI) water. Parafilm covers were applied all around the vein to restrict the evaporation of water molecules through secondary pathways, directly from the container. A digital photo of the same is shown in the inset of Figure 1g. The evaporation behavior was monitored by measuring the weight change of the ampoule at a consistent interval of time. The experiment was performed in a controlled environment (inside a stainless steel chamber (diameter, 27 cm; height, 30 cm); Supporting Figure S6) with controlled RH, temperature, light intensity, and wind velocity. Evaporation rates ($E.R._{vein}$) through the midrib vein under different conditions were calculated by employing eq 1.

$$E.\ R._{vein} = \frac{\text{change in weight (kg)}}{\text{evaporating area (m}^2\text{)} \times \text{time (h)}} \quad (1)$$

where the circumference (A) of the isolated midrib vein exposed to the atmosphere was considered as the evaporating area. It was determined by assuming the vein to be an oval-shaped cylinder (in the inset of Figure 1b). The diameter was measured along two perpendicular lines, or axes at two positions, at the tip of the exposed midrib vein and at the bottom just above the parafilm cover. L is the length of the vein above the parafilm cover. The details of the calculation of evaporating area are discussed in Supporting Figure S7. In Figure 1g, the water evaporation rate through the raw leaf vein and extracted leaf vein via the digestion process is compared with that of a similar ampoule minus the vein structure. Remarkably, even under dark conditions, inside a stainless steel chamber (30% RH and 25 °C), the $E.R._{vein}$ value was found to be 1.5 $kg{\cdot}m^{-2}{\cdot}h^{-1}$, which is nearly 50 times higher than a similar ampoule covered with a parafilm having a hole similar to the diameter of the vein structure.

The incredible evaporation process through the vein of a naked leaf can be subdivided into two steps. The first step involves transportation of water molecules from the container to the evaporating surface through hierarchal capillaries of the natural leaf vein. In the second step, the transported water molecules diffuse and/or evaporate into the surrounding atmosphere. With a view to find out the rate-determining step, the evaporation rate through the leaf vein was studied by varying the parameters of the surrounding atmosphere (like relative humidity (RH), temperature, and wind velocity). As shown in Figure 2a, the rate of evaporation through the naked leaf vein was found to be dependent on the atmospheric humidity levels,

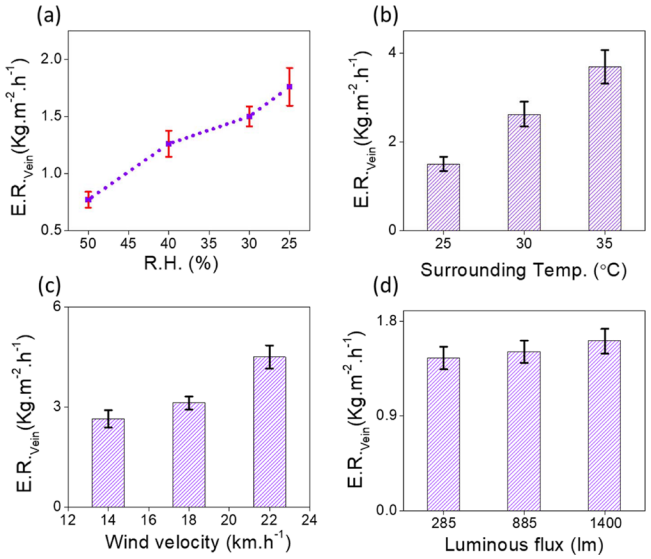

Figure 2. Evaporation through isolated leaf veins. $E.R._{vein}$ of DI water through an isolated midrib vein with varying (a) relative humidity levels, (b) atmospheric temperatures, (c) wind velocities, and (d) light intensities under controlled environmental conditions. To study the dependence of $E.R._{vein}$ on a particular parameter, the remaining parameters were fixed at 30% RH, 25 °C, 50 lux, and 0.54 $km{\cdot}h^{-1}$.

which was varied by employing a combination of calcium chloride desiccant inside a closed chamber and control flow of warm N_2 gas. A schematic of the experimental chamber is shown in Supporting Figure S6. With decreasing humidity level, the $E.R._{vein}$ value was found to be increased from 0.77 $kg{\cdot}m^{-2}{\cdot}h^{-1}$ at 50% RH to 1.76 $kg{\cdot}m^{-2}{\cdot}h^{-1}$ at 25% RH (see Figure 2a). The enhancement in the evaporation rate with decreasing humidity level suggests that the rate-determining step involves diffusion and evaporation of the transported water molecules from the capillary mouth into the air atmosphere, which is also called the kinetic-limited evaporation process. The dependence of humidity in the kinetic-limited evaporation process is attributed to the increasing difference between the partial pressure and vapor pressure of the water molecules. The occurrence of the kinetic-limited evaporation process was also supported by a drastic improvement in the $E.R._{vein}$ values with increasing atmospheric temperature (the bar diagram in Figure 2b). In the kinetic-limited evaporation process, the elevated atmospheric temperature aids in the evaporation process by increasing both the kinetic energy of the molecules and the saturation vapor density of the atmosphere. A similar escalation in the evaporation rates through the naked leaf vein was also observed with increasing air velocity of the surrounding environment. Figure 2c shows the bar diagram of $E.R._{vein}$ values calculated for the leaf vein at different air velocities created by a domestic table fan under dark conditions. The decreasing boundary layer at the evaporating surface with increasing air velocity creates a conducive environment for the mass transfer, which in turn leads to the remarkable enhancement in the evaporation rate.

One of the prerequisite of the kinetic-limited evaporation process is the seamless supply of water molecules from the reservoirs to the evaporating surface, which require a tremendous flow rate of water through the capillary channels of naked leaf veins. In natural leaf veins, the fiber tracheids and

https://doi.org/10.1021/acsomega.1c02398
ACS Omega 2021, 6, 20379−20387

vessels, collectively called microchannels, are the major conduits for water transportation. The digestive process consumes the lignin embedded in the cellulose and hemicellulose matrices of the leaf vein and generates numerous hydrophilic nanochannels among the microfiber tracheids.[20] These newly generated hydrophilic nanochannels, previously occupied by hydrophobic lignin, provide an additional means for fluid transport by increasing the hydrophilicity and available surface area. The occurrence of numerous nanopores in the dignified leaf can be verified from the BET surface area and BJH pore distribution analysis, where the leaf vein possesses a high surface area of approximately 240 $m^2 \cdot g^{-1}$. The observed smaller pore distribution shown in Supporting Figure S8 can be attributed to the presence of nanopores.[21] These inherent microchannels with low tortuosity and open structures are oriented along the growth direction, resulting in efficient mass transport in the upward direction as shown in the schematic diagram of Figure 3a. Moreover, some small pits with an average diameter of ∼1

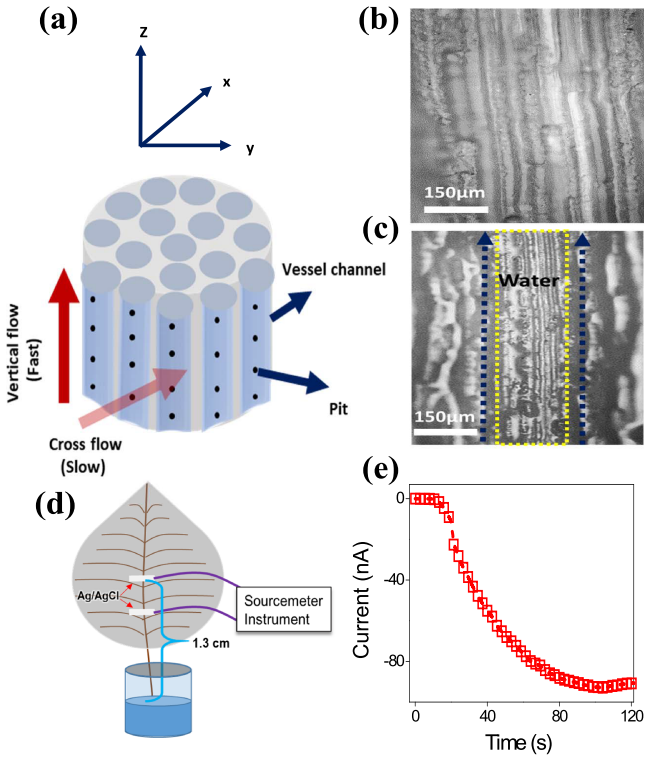

Figure 3. Mechanism of water transportation. (a) Schematic diagram showing anisotropic water transportation through the vessel channels and the interconnected pits in a leaf midrib vein. Optical microscopic images of a leaf midrib vein (b) before and (c) after water transportation, showing an upward flow of water along the growth direction. (d) Schematic illustration of the experimental setup used for the measurement of the water transport velocity through naked leaf veins. (e) Development of ionic current as a function of time between the Ag/AgCl electrodes installed at the midrib vein after dipping the base into liquid DI water.

μm are present on the internal surface of the microchannels, which enable transverse mass transport between the adjacent vessels.[22,23]

The porous leaf vein with numerous aligned hydrophilic micro- and nanochannels can effectively transport water molecules from the bottom to the evaporating surface, maintaining a continuous network of water channels throughout the vein structure. As water molecules evaporate from the upper surface, it is simultaneously compensated by capillary-induced pumping from the bottom through the vessels and other interconnected channels in the leaf vein, ensuring an uninterrupted supply of water molecules for the evaporation process. The negative pressure at the top of the open veins that originated from water evaporation induces a large capillary force inside the micro- and nanosized channels of the leaf vein.[22−24] Water molecules can also flow in the transverse direction in between the adjacent vessels channels via the interconnected pits (Figure 3a). However, this transverse flow occurs via slow diffusion from one vessel to another instead of free liquid advection, and hence, the pits have little impact on water transport along the vessels in the vertical direction, but it contributes toward an overall evaporation process from the outer surface.[22,25] The upward water transportation along the growth direction can be visualized from optical microscopic investigation shown in Figure 3b,c. The water transportation process along the growth direction was recorded under optical microscopic investigation as shown in Supporting Movie 1. The transposition of water along the growth direction of the leaf midrib vein was also traced by using an aqueous Eriochrome black T solution, shown in Supporting Figure S9.

To study the water transport velocity from the reservoirs to the evaporating surface through capillary channels of naked leaf veins, two Ag/AgCl electrodes were mounted on the midrib vein of a naked vein network at a distance of 7 mm apart (see the schematic of Figure 3d). To detect the development of the ionic current, both these electrodes were connected to a sourcemeter instrument. As the cellulose-based leaf veins are electrically insulating, under dry conditions, no detectable current was observed. Once the base of the midrib vein touched the water surface, the water molecules started moving toward the vein network through the midrib vein. As soon as the vein between the electrodes got wetted, a sudden increase in the current value was detected. The ionic current thus recorded by the sourcemeter instrument is plotted as a function of time (Figure 3e). The time lag between the midrib vein touching the water surface and the appearance of ionic current at the sourcemeter instrument was taken as the time (t = 9 s) required by the water molecules to travel the distance (x = 1.3 cm). Accordingly, the water transport velocity was calculated to be 1444 $\mu m \cdot s^{-1}$. Just for comparison, the spider silk and cactus spine exhibit water transport velocities of ∼30 and ∼12 $\mu m \cdot s^{-1}$, respectively.[26,27] Li *et al.* measured the flow velocity of water in ultrathin graphene nanocapillaries to be ∼100,000 $\mu m \cdot s^{-1}$.[2] Similarly, the velocity of water on the *Sarracenia* trichome is reported to be ∼11,738 $\mu m \cdot s^{-1}$.[27] The diffusivity of water (D) through the midrib vein was calculated to be $D = 3.1 \times 10^6$ $\mu m^2 \cdot s^{-1}$ by using Einstein's approximation for three-dimensional diffusions (eq 2).[28−30]

$$x^2 = 6Dt \tag{2}$$

Typically, the theoretical limit of the kinetic-limited evaporation flux (m_k'') is predicted by the classical H−K eq 3.

$$m_k'' = \left(\frac{M}{2\pi R}\right)^{1/2}\left(\sigma_e \frac{P_{v,eq}}{\sqrt{T_i}} - \sigma_c \frac{P_v}{\sqrt{T_v}}\right) \tag{3}$$

where M is the molar mass of water, and R is the universal gas constant. σ_e is the evaporation coefficient, the fraction of molecules that strike the interface and change the phase from the liquid to vapor state (typical values varies between 1 and 0.001).[5] σ_c is the condensation coefficient, the fraction of

https://doi.org/10.1021/acsomega.1c02398
ACS Omega 2021, 6, 20379−20387

molecules that strike the interface and change the phase from the vapor to liquid state (typically varies between 1 and 0.001).[5] $P_{v,eq}$ is the equilibrium vapor pressure of the liquid at the interface, P_v is the partial pressure of the vapor in the gas phase calculated from the relative humidity of the experimental condition (RH = $P_v/P_{v,eq}$). T_i is the temperature of the liquid (the temperature of the evaporating area of the vein measured by a noncontact IR camera), and T_v is the vapor temperature (measured by a thermometer at a distance of 10 mm from the vein).

The kinetic-limited evaporation flux calculated by the H−K equation, considering the current experimental conditions, was found to be 2.5 kg·m^{-2}·h^{-1} (considering both σ_e and σ_c to be 0.001),[5] which is in the same order of magnitude with the experimental results. The experimental evaporation rate at 25 °C corresponds to a heat flux of 0.08 W/cm^2, which is easily achievable under the current experimental conditions. Similarly, the velocity of water vapor leaving the interface from the volumetric flux was calculated to be 20 mm·s^{-1}, which is several times smaller than that of the RMS velocities of vapor at the same temperature.

To the best of our knowledge, the E.R.$_{vein}$ value recorded with the midrib vein inside an indoor environment with an RH of 30% and a temperature of 25 °C is on a par with the recently published evaporation rates for the solar steam generators under intense simulated sunlight (1 sun or higher). For reference, in Supporting Table 1, the evaporation rates of some of the recently reported solar steam generators are compared with that of the E.R.$_{vein}$ value. Moreover, the naked leaf veins are deprived of any photothermal materials. The evaporation rate through the leaf vein was also studied at different light intensities by employing LED light of different luminous fluxes. As can be seen from the bar diagram in Figure 2d, the E.R.$_{vein}$ value does not alter significantly with increasing luminous flux of the employed LEDs; the slight variation in E.R.$_{vein}$ can be attributed to the little rise in temperature of the surrounding atmosphere. So, it can be argued that in direct contrast to the solar steam generators, the naked leaf vein exhibits remarkable evaporation rates even in the absence of light.

The amount of water evaporating through the midrib vein can be further improved by keeping a definite portion of the vein network at their natural position. A photo of the same is shown in Figure 4a. When the mass lost from the glass bottle was normalized by the circumference of the midrib vein, it yielded remarkable values of E.R.$_{vein}$. For example, with a vein network of 6 cm^2 area, the E.R.$_{vein}$ was calculated to be 8.34 kg·m^{-2}·h^{-1} (30% RH and 25 °C). However, when the evaporation rate was normalized by the total area covered by the vein network (E.R.$_{network}$), it yielded a humble value of evaporation rate (~0.25 kg·m^{-2}·h^{-1}). Large void spaces in the vein network area and the small cross section of the midribs that connect the vein network with the water reservoirs are believed to be the reason behind the humble E.R.$_{network}$ values. However, it is worth noting that even though, in the presence of an extended network area, the value of evaporation rate is lower, the actual mass of water evaporating through the veins is higher than that of the isolated midrib vein. Therefore, the midrib vein with the extended vein network will be more beneficial for the practical applications.

The extraordinary ability of naked leaf veins extracted from fallen tree leaves to evaporate water at an expedited rate under ambient conditions could find multiple technological applications in areas like water desalination, harvesting of exquisite salts or molecules, humidification, and energy conversion. As a proof of concept, here, we have studied the evaporation of water

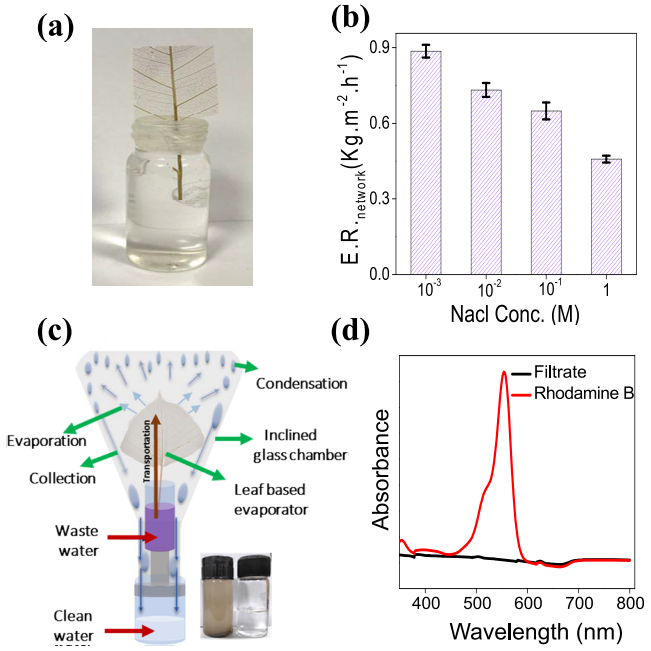

Figure 4. Application of isolated leaf veins. (a) Digital photo of the E.R.$_{network}$-based evaporating system, where midrib veins are extended with a definite portion (6 cm^2) of the venation network. (b) E.R.$_{network}$ values through a naked vein network with varying salt concentrations under 35 °C atmospheric temperature and 30% RH. (c) Schematic illustration of the experimental setup used for condensing the molecules evaporating from waste water (mud water, seawater, and dye solution) through the naked vein network. The inset shows a photo of mud water before and after evaporation. (d) UV−Vis spectra and digital photos of rhodamine B (0.01 M) solution before and after evaporation through the vein network.

molecules from saltwater by employing midrib veins with an extended vein network (area, 6 cm^2). Figure 4b shows the E.R.$_{network}$ values as a function of NaCl concentration at an elevated room temperature of 35 °C and 30% RH. The decreasing evaporation rate with increasing salt concentration is attributed to the increase in the osmotic pressure that needs to be overcome by the evaporating water molecules. Such evaporation of water molecules from the salt solutions would be suitable for applications like water desalination or wastewater treatment. As a proof of concept, an experimental setup was designed to collect the water molecules evaporating from the wastewater samples; a schematic illustration of the same is shown in Figure 4c. As shown in Supporting Figure S10, the midrib of a naked vein network (area, 13 cm^2) was immersed into a solution of simulated seawater (0.6 M NaCl) inside a glass chamber, where except the collection chamber (at the bottom), the entire setup was exposed to direct sunlight on a bright sunny day (the temperature and light intensity were recorded to be 30 °C and ~77 × 10^3 lux, respectively). Parafilm covers were applied in the vials all around the vein structures to limit the evaporation of water molecules through secondary pathways. Remarkably, within 5 h of the experiment, ~5 mL of clean water was collected at the water collection chamber. However, after 48 h of operation time, salt molecules tend to deposit on the surface of the leaf evaporator as shown in Supporting Figure S11, resulting in the reduction of the E.R. value. But the accumulated salts can be removed via simple physical shaking or by washing with water, and removal of salts via a washing process did not seem to have a significant impact on the evaporation efficiency of

https://doi.org/10.1021/acsomega.1c02398
ACS Omega 2021, 6, 20379−20387

the leaf-based evaporator. The experiment was also repeated with solutions of muddy water and 0.01 M rhodamine B dye (inset of Figure 4c). The water samples collected from concentrated salt and dye solutions did not show any salt or dye ions in the detectable range. The UV−Vis spectra and digital photos of the dye solutions before and after evaporation through the vein network are shown in Figure 4d. Steam generation through a naked leaf vein could have several advantages over the solar steam generator. For example, in the solar steam generation, photothermal materials are employed to convert sunlight into heat, which in turn induces rapid evaporation of the surrounding water molecules.[31,32] While solar steam generation is one of the most promising methods of treating water in an environment-friendly manner, the involvement of the photothermal materials complicates the process. The complication with photoactive material-based devices arises from exclusive requirements such as homogeneous exposure of light throughout the photoactive material, thermal insulation between the active material and bulk liquid, and periodic removal of the deposited salts to avoid blocking of light and capillary pores.[33,34] No such complication would occur in the case of nonsolar steam generation through naked leaf veins.

Leaf veins are made of dense micro- and nanofibrils bearing negative surface charges, and such charges on the walls of tiny channels possess the ability to break the electrical neutrality of electrolytes flowing through it.[35−39] This property of the minuscule biochannels is exploited here to harvest electrical energy through the electrokinetic streaming potential. As a proof of concept, two Ag/AgCl electrodes were installed in the midrib vein of a vein network (area, 13 cm^2) at a distance of 7 mm apart. As soon as the base of the midrib vein was immersed into liquid water, a constant flow of water molecules occurs through the channels of the midrib vein. The rapid evaporation in the vein network is the driving force behind this uphill flow of liquid water. The flow of DI water generated an open-circuit potential of 120 mV between the two Ag/AgCl electrodes installed along the midrib vein (Figure 5a). Further, the potential generated by water transportation can be easily controlled by tuning the evaporation rate. For example, exposure of halogen light (at 30 °C) drastically improved the evaporation rate from 0.133 kg·m^{-2}·h^{-1} to 2.1 kg·m^{-2}·h^{-1}, and concomitant with this enhanced evaporation rate, the open-circuit potential was also improved from 120 mV to 280 mV, shown in Figure 5a. As soon as the light was put off, the voltage went down to original values and these cycles of controlling the output voltage by applying light/heat energy can be repeated multiple times (see Figure 5b). The experiment of streaming potential generation was also repeated with salt solutions of different concentrations (10^{-6} to 1 M). As shown in Figure 5c, the plot of salt concentrations vs open-circuit voltage shows two distinct characteristic regimes. In the low-concentration regime (10^{-6} to 10^{-2} M), the voltage increases with increasing salt concentration, but in the high-concentration regime (10^{-2} to 1 M), it decreases with increasing salt concentration. To understand this behavior, a nanofluidic device of an isolated midrib vein was constructed by immersing the same in a freshly prepared PDMS elastomer. Figure 5d shows representative current−voltage (I−V) curves measured through a leaf vein-based nanofluidic device. As presented in Figure 5e, the biochannels of the leaf vein exhibit the characteristic surface charge-governed ionic conductivity of nanofluidic channels. Comparison of the curves in Figure 5d,e suggests that in the low-concentration regime (10^{-6} to 10^{-2} M), where transport of the ions is controlled by the surface charges of

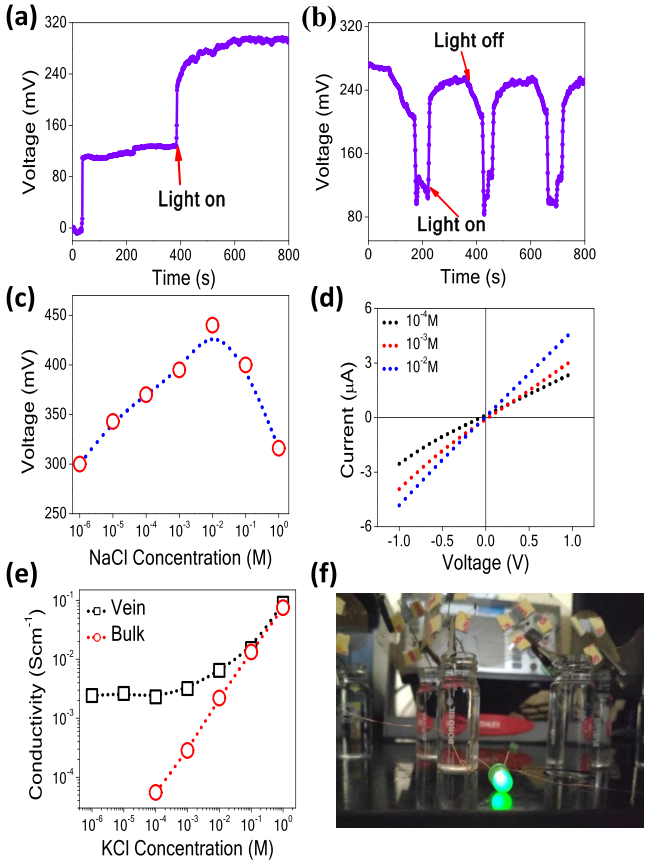

Figure 5. Streaming potential through naked leaf veins. (a) Plot of open-circuit potential generated by the water molecules streaming through the leaf veins as a function of time. Exposure of halogen light (intensity, 10^4 lux; at 30 °C) drastically improves the evaporation rate (from 0.133 to 2.5 kg·m^{-2}·h^{-1}), and a concomitant enhancement is also reflected in the values of open-circuit potential. (b) Tuning of open-circuit voltage of a leaf vein by the exposure of halogen light (intensity, 10^4 lux; at 30 °C) in repetitive cycles. (c) Open-circuit voltage of leaf veins as a function of the NaCl concentration in the water reservoir. (d) Current−voltage (I−V) curves and (e) ionic conductivity as a function of KCl concentration through the nanofluidic device of an isolated midrib vein. The vein-based nanofluidic device shows the typical characteristics of surface charge-governed ionic conductivity. (f) Application of streaming potential generated in the leaf vein to power an LED (3 V).

the biochannels, the open-circuit voltage increases with increasing concentration of the ionic species. On the other hand, in the high-concentration regime (10^{-2} to 1 M), the increasing salt concentrations increase the shielding of negative surface charges. As a result, the effectiveness of the surface charges in breaking the charge neutrality decreases, and concomitantly, the magnitude of the open-circuit potential decreases.[40−42] The voltage generated from the solutions streaming through the leaf veins can also be used to carry out useful works such as lighting of an LED. Figure 5f shows lighting of a 3 V LED by connecting 10 leaf vein network-based streaming energy-harvesting devices in series (Supplementary Movie 2).

CONCLUSIONS

In conclusion, we have demonstrated that the veins of a natural leaf exhibit remarkable evaporation efficiency under ambient conditions. The evaporation rates can be further improved by

https://doi.org/10.1021/acsomega.1c02398
ACS Omega 2021, 6, 20379−20387

tuning the environmental conditions like temperature, humidity, and wind speed. Even in the dark conditions, with the help of air flow, naked leaf veins exhibit an evaporation rate on a par with the best photothermal material-based solar steam generators under intense light (1 sun). Materials with such a high evaporation rate could find multiple applications in areas like water desalination, harvesting of streaming potential, harnessing of exquisite salts and molecules, and humidification. The isolated leaf veins can be an ideal host for photothermal materials like plasmonic nanoparticles or carbon-based nanomaterials to develop solar steam generators with exceptional evaporation rates. Looking at the variety and abundance, the vein-based evaporator could provide an ideal platform for futuristic water treatment and energy-harvesting devices.

METHODS

Extraction of the Vein Network from a Natural Leaf. To extract veins of a natural leaf in its naked form, a collection of aged and fallen leaves (typically 60 in number) of Peepal tree (*F. religiosa*) was immersed into a tap water-filled closed container (25 L) for about 25 days. After 25 days, the upper epidermis and mesophyll layers of the leaf blade turned into a soft, smelly, and brownish-colored loosely bound material. The network of naked leaf veins (shown in Figure 1a) was obtained after gently removing those loosely bound materials by using a soft nylon brush. The as-obtained vein network was dried by using a heat gun (approximate temperature, ∼50 °C).

Evaporation of Water through Leaf Veins. For the evaporation experiment, glass ampoules containing 15 mL of deionized water were first sealed with a parafilm cover. The parafilm sealing was pierced with the help of a needle to immerse the isolated midrib part of the naked leaf vein systems. Glass ampoules containing the naked vein network were kept in a controlled environment (30%, RH, 25 °C, 50 lux, and 0.54 km·h^{-1}) for a recorded amount of time. The evaporated amount of water through the midrib vein was gravimetrically estimated by measuring the weight change of the ampoule at consistent intervals of time. To study the effect of temperature on evaporation rates, naked veins immersed in glass ampoules were kept at a fixed distance from the heater under a controlled environment with RH and airflow rate measured to be 30% and 0.54 km·h^{-1}, respectively. Thermometer, digital lux meter, thermo-hygrometer, and thermal anemometer instruments were installed at the same levels of the vein network to record the respective parameters in real time. Similarly, for the measurements of the evaporation rate under varying humidity conditions, the humidity level of the chamber was varied by using a combination of the required amounts of desiccants (calcium chloride) inside the chamber and warm N_2 flow. Dependence of the evaporation rate on the airflow velocity was studied by using a domestic table fan. LED light with different luminous fluxes was employed to study the evaporation rate under varying light intensities.

Water Diffusivity Experiment. An ampoule containing 15 mL of DI water was sealed with a parafilm, and a small hole was pierced through the parafilm to insert the midrib part of an isolated vein network. Two Ag/AgCl electrodes (7 mm apart) were installed to the midrib of the naked vein network (area, 13 cm^2) by applying conductive silver paste. The electrodes were attached to a sourcemeter instrument (Keithley 2450), and the development of current values as a function of time (time interval of 1.33 s) was recorded.

Surface Charge-Governed Ionic Transport. The nanofluidic device of the naked leaf vein was prepared by embedding an isolated midrib (dimension, 20 mm × 1 mm × 0.3 mm) into a freshly prepared blend of polydimethylsiloxane (PDMS) prepolymer and curing agent. Once the PDMS stub was fully cured, two reservoirs of 0.4 mL volume were carved out at both ends of the midrib to expose the same into electrolyte solutions. Electrical measurements were carried out by employing a sourcemeter instrument connected with two Ag/AgCl electrodes, which were immersed into the reservoirs filled with electrolyte solutions of different concentrations (from 10^{-6} M to 1 M). Conductance values (G) at different electrolyte concentrations were calculated from the slope of the $I-V$ curves recorded by sweeping the voltage from −1 V to 1 V. The following equation was used for the calculations of conductivity values (C): $C = G \times$ cell constant.

Characterizations. The microstructure of the naked leaf vein was characterized by employing optical (Olympus BX51) and field emission scanning electron microscopes (Zeiss; model: Sigma). Spectroscopic techniques such as UV−Vis spectroscopy (PerkinElmer; model: Lambda 750) and Fourier transform infrared spectroscopy (PerkinElmer IR spectrometer) were used for the characterization of the vein network. The light intensity was measured using a digital lux meter (model: LX1330B). The relative humidity, temperature, and wind speed of the surrounding environment were measured using thermo-hygrometer (testo 605i), thermometer, and thermal anemometer (testo 405i) instruments. All the electrochemical measurements were performed with the help of a sourcemeter instrument (Keithley 2450 model). Dye separation experiments were studied by using a UV−Vis spectrophotometer (Systronics; model: 117).

ASSOCIATED CONTENT

Supporting Information

The Supporting Information is available free of charge at https://pubs.acs.org/doi/10.1021/acsomega.1c02398.

IR and DRS spectra of a naked vein network, cross-sectional optical microscopic image of a vein network, optical microscopic and FESEM characterization of a naked vein network, setup used for clean water harvesting by evaporation through the naked vein network from contaminated water systems, details of calculation of the evaporating area of the leaf-based evaporator, and BJH pore size distribution in a leaf midrib vein (PDF)

Clip showing the water transportation process along the growth direction (MP4)

Clip showing lighting of an LED connecting 10 leaf vein network-based streaming energy-harvesting devices in series (MP4)

AUTHOR INFORMATION

Corresponding Author

Kalyan Raidongia − *Department of Chemistry and Centre for Nanotechnology, Indian Institute of Technology Guwahati, Guwahati 781039 Assam, India;* orcid.org/0000-0001-7829-7498; Email: k.raidongia@iitg.ac.in

Authors

Tukhar Jyoti Konch − *Department of Chemistry, Indian Institute of Technology Guwahati, Guwahati 781039 Assam, India*

Trisha Dutta − *Department of Chemistry, Indian Institute of Technology Guwahati, Guwahati 781039 Assam, India*
Madhurjya Buragohain − *Department of Chemistry, Indian Institute of Technology Guwahati, Guwahati 781039 Assam, India*

Complete contact information is available at: https://pubs.acs.org/10.1021/acsomega.1c02398

Author Contributions

[§]T.J.K. and T.D. contributed equally to this work.

Author Contributions

K.R. conceived the concept and designed the experiments. T.D., T.J.K., and M.B. performed the experiments and analyzed the data. K.R., T.D., and T.J.K. wrote the paper, with input from all the authors. All authors approved the final version of the manuscript.

Notes

The authors declare no competing financial interest.

■ ACKNOWLEDGMENTS

K.R. acknowledges the EMR grant of CSIR-India (01(2984)/19/EMR-II) and Core Research Grant of SERB (CRG/2020/002943) of the Science and Engineering Research Board (SERB), India, for financial support. All the authors thank CIF-IIT Guwahati, DST-FIST-Chemistry at IIT Guwahati for the help with sample characterizations and Ankita Goswami for her help toward the extraction of the vein network. T.D. and T.J.K. are grateful to IITG for Ph.D. fellowships.

■ REFERENCES

(1) Zhang, X.; Liu, H.; Jiang, L. Wettability and Applications of Nanochannels. *Adv. Mater.* **2019**, *31*, 1804508.
(2) Li, Y.; Alibakhshi, M. A.; Zhao, Y.; Duan, C. Exploring Ultimate Water Capillary Evaporation in Nanoscale Conduits. *Nano Lett.* **2017**, *17*, 4813−4819.
(3) Radha, B.; Esfandiar, A.; Wang, F. C.; Rooney, A. P.; Gopinadhan, K.; Keerthi, A.; Mishchenko, A.; Janardanan, A.; Blake, P.; Fumagalli, L.; Lozada-Hidalgo, M.; Garaj, S.; Haigh, S. J.; Grigorieva, I. V.; Wu, H. A.; Geim, A. K. Molecular Transport Through Capillaries Made with Atomic-scale Precision. *Nature* **2016**, *538*, 222−225.
(4) Gimenez, R.; Soler-Illia, G. J. A. A.; Berli, C. L. A.; Bellino, M. G. Nanopore-Enhanced Drop Evaporation: When Cooler or More Saline Water Droplets Evaporate Faster. *ACS Nano* **2020**, *14*, 2702−2708.
(5) Persad, A. H.; Ward, C. A. Expressions for the Evaporation and Condensation Coefficients in the Hertz-Knudsen Relation. *Chem. Rev.* **2016**, *116*, 7727−7767.
(6) Narayanan, S.; Fedorov, A. G.; Joshi, Y. K. Interfacial Transport of Evaporating Water Confined in Nanopores. *Langmuir* **2011**, *27*, 10666−10676.
(7) Wu, X.; Chen, G. Y.; Zhang, W.; Liu, X.; Xu, H. A Plant-Transpiration-Process-Inspired Strategy for Highly Efficient Solar Evaporation. *Adv. Sustainable Syst.* **2017**, *1*, 1700046.
(8) Steudle, E. Water Uptake by Roots: Effects of Water Deficit. *J. Exp. Bot.* **2000**, *51*, 1531−1542.
(9) P. S., Nobel *Physicochemical and Environmental Plant Physiology*; *pp.* 635 (Academic Press, Inc.: San Diego, CA. 1991).
(10) Zhou, H.; Li, X.; Fan, T.; Osterloh, F. E.; Ding, J.; Sabio, E. M.; Zhang, D.; Guo, Q. Artificial Inorganic Leafs for Efficient Photochemical Hydrogen Production Inspired by Natural Photosynthesis. *Adv. Mater.* **2010**, *22*, 951−956.
(11) Coté, G. G.; Gibernau, M. Distribution of Calcium Oxalate Crystals in Floral Organs of Araceae in Relation to Pollination Strategy. *Am. J. Bot.* **2012**, *99*, 1231−1242.
(12) Han, B.; Huang, Y.; Li, R.; Peng, Q.; Luo, J.; Pei, K.; Herczynski, A.; Kempa, K.; Ren, Z.; Gao, J. Bio-Inspired Networks for Optoelectronic Applications. *Nat. Commun.* **2014**, *5*, 1−7.
(13) Kim, H. K.; Park, J.; Hwang, I. Investigating Water Transport through the Xylem Network in Vascular Plants. *J. Exp. Bot.* **2014**, *65*, 1895−1904.
(14) Wu, M.-B.; Hong, Y.-M.; Liu, C.; Yang, J.; Wang, X.-P.; Agarwal, S.; Greiner, A.; Xu, Z.-K. Delignified Wood with Unprecedented Anti-Oil Properties for the highly efficient Separation of Crude Oil/Water Mixtures. *J. Mater. Chem. A* **2019**, *7*, 16735−16741.
(15) Yang, T.; Cao, J.; Ma, E. How does delignification influence the furfurylation of wood? *Ind. Crops Prod.* **2019**, *135*, 91−98.
(16) Wu, J.; Wu, Y.; Yang, F.; Tang, C.; Huang, Q.; Zhang, J. Impact of Delignification on Morphological, Optical and Mechanical Properties of Transparent Wood. *Composites, Part A* **2019**, *117*, 324−331.
(17) Khakalo, A.; Tanaka, A.; Korpela, A.; Orelma, H. Delignification and Ionic Liquid Treatment of Wood toward Multifunctional High-Performance Structural Materials. *ACS Appl. Mater. Interfaces* **2020**, *12*, 23532−23542.
(18) Li, Z.; Chen, C.; Mi, R.; Gan, W.; Dai, J.; Jiao, M.; Xie, H.; Yao, Y.; Xiao, S.; Hu, L. A Strong, Tough, and Scalable Structural Material from Fast-Growing Bamboo. *Adv. Mater.* **2020**, *32*, 1906308.
(19) Hou, D.; Li, T.; Chen, X.; He, S.; Dai, J.; Mofid, S. A.; Hou, D.; Iddya, A.; Jassby, D.; Yang, R.; Hu, L.; Ren, Z. J. Hydrophobic nanostructured wood membrane for thermally efficient distillation. *Sci. Adv.* **2019**, *5*, No. eaaw3203.
(20) Chen, X.; Zhu, X.; He, S.; Hu, L.; Ren, Z. J. Advanced Nanowood Materials for the Water-Energy Nexus. *Adv. Mater.* **2020**, 2001240.
(21) Wu, Y.; Zhou, J.; Huang, Q.; Yang, F.; Wang, Y.; Wang, J. Study on the properties of partially transparent wood under different delignification processes. *Polymer* **2020**, *123*, 661−675.
(22) Jia, C.; Jiang, F.; Hu, P.; Kuang, Y.; He, S.; Li, T.; Chen, C.; Murphy, A.; Yang, C.; Yao, Y.; Dai, J.; Raub, C. B.; Luo, X.; Hu, L. Anisotropic, Mesoporous Microfluidic Frameworks with Scalable, Aligned Cellulose Nanofibers. *ACS Appl. Mater. Interfaces* **2018**, *10*, 7362−7370.
(23) Jia, C.; Li, Y.; Yang, Z.; Chen, G.; Yao, Y.; Jiang, F.; Kuang, Y.; Pastel, G.; Xie, H.; Yang, B.; Das, S.; Hu, L. Rich Mesostructures Derived from Natural Woods for Solar Steam Generation. *Joule* **2017**, *1*, 588−599.
(24) Zhu, M.; Li, Y.; Chen, G.; Jiang, F.; Yang, Z.; Luo, X.; Wang, Y.; Lacey, S. D.; Dai, J.; Wang, C.; Jia, C.; Wan, J.; Yao, Y.; Gong, A.; Yang, B.; Yu, Z.; Das, S.; Hu, L. Tree-Inspired Design for High-Efficiency Water Extraction. *Adv. Mater.* **2017**, *29*, 1704107.
(25) Chen, F.; Gong, A. S.; Zhu, M.; Chen, G.; Lacey, S. D.; Jiang, F.; Li, Y.; Wang, Y.; Dai, J.; Yao, Y.; Song, J.; Liu, B.; Fu, K.; Das, S.; Hu, L. Mesoporous, Three-Dimensional Wood Membrane Decorated with Nanoparticles for Highly Efficient Water Treatment. *ACS Nano* **2017**, *11*, 4275−4282.
(26) Zheng, Y.; Bai, H.; Huang, Z.; Tian, X.; Nie, F. Q.; Zhao, Y.; Zhai, J.; Jiang, L. Directional Water Collection on Wetted Spider Silk. *Nature* **2010**, *463*, 640−643.
(27) Ju, J.; Bai, H.; Zheng, Y.; Zhao, T.; Fang, R.; Jiang, L. A Multi-Structural and Multi-Functional Integrated fog Collection System in Cactus. *Nat. Commun.* **2012**, *3*, 1−6.
(28) Einstein, A. Über die von der molekularkinetischen Theorie der Wärme geforderte Bewegung von in ruhenden Flüssigkeiten suspendierten Teilchen. *Ann. Phys.* **1905**, *322*, 549.
(29) Konch, T. J.; Gogoi, R. K.; Gogoi, A.; Saha, K.; Deka, J.; Reddy, K. A.; Raidongia, K. Nanofluidic Transport Through Humic acid Modified Graphene Oxide Nanochannels. *Mater. Chem. Front.* **2018**, *2*, 1647−1654.
(30) Konch, T. J.; Bora, A. P.; Raidongia, K. Disposable Fluidic Devices of Bionanochannels for Enzymatic Monitoring and Energy Harvesting. *ACS Appl. Bio Mater.* **2019**, *2*, 2549−2556.
(31) Jiang, F.; Liu, H.; Li, Y.; Kuang, Y.; Xu, X.; Chen, C.; Huang, H.; Jia, C.; Zhao, X.; Hitz, E.; Zhou, Y.; Yang, R.; Cui, L.; Hu, L. Lightweight, Mesoporous, and Highly Absorptive All-Nanofiber

Aerogel for Efficient Solar Steam Generation. *ACS Appl. Mater. Interfaces* **2018**, *10*, 1104−1112.
(32) Lin, Y.; Xu, H.; Shan, X.; Di, Y.; Zhao, A.; Hu, Y.; Gan, Z. Solar Steam Generation Based on the Photothermal Effect: From Designs to Applications, and beyond. *J. Mater. Chem. A* **2019**, *7*, 19203−19227.
(33) He, S.; Chen, C.; Kuang, Y.; Mi, R.; Liu, Y.; Pei, Y.; Kong, W.; Gan, W.; Xie, H.; Hitz, E.; Jia, C.; Chen, X.; Gong, A.; Liao, J.; Li, J.; Ren, Z. J.; Yang, B.; Das, S.; Hu, L. Nature-Inspired Salt Resistant Bimodal Porous Solar Evaporator for Efficient and Stable Water Desalination. *Energy Environ. Sci.* **2019**, *12*, 1558−1567.
(34) Ni, G.; Zandavi, S. H.; Javid, S. M.; Boriskina, S. V.; Cooper, T. A.; Chen, G. A Salt-Rejecting Floating Solar Still for Low-Cost Desalination. *Energy Environ. Sci.* **2018**, *11*, 1510−1519.
(35) Li, T.; Li, S. X.; Kong, W.; Chen, C.; Hitz, E.; Jia, C.; Dai, J.; Zhang, X.; Briber, R.; Siwy, Z.; Reed, M.; Hu, L. A Nanofluidic Ion Regulation Membrane with Aligned Cellulose Nanofibers. *Sci. Adv.* **2019**, *5*, No. eaau4238.
(36) Li, T.; Zhang, X.; Lacey, S. D.; Mi, R.; Zhao, X.; Jiang, F.; Song, J.; Liu, Z.; Chen, G.; Dai, J.; Yao, Y.; Das, S.; Yang, R.; Briber, R. M.; Hu, L. Cellulose Ionic Conductors with High Differential Thermal Voltage for Low-Grade Heat Harvesting. *Nat. Mater.* **2019**, *18*, 608−613.
(37) Das, S. S.; Pedireddi, V. M.; Bandopadhyay, A.; Saha, P.; Chakraborty, S. Electrical Power Generation from Wet Textile Mediated by Spontaneous Nanoscale Evaporation. *Nano Lett.* **2019**, *19*, 7191−7200.
(38) Yin, J.; Li, X.; Yu, J.; Zhang, Z.; Zhou, J.; Guo, W. Generating Electricity by Moving a Droplet of Ionic Liquid Along Graphene. *Nat. Nanotechnol.* **2014**, *9*, 378−383.
(39) Xue, G.; Xu, Y.; Ding, T.; Li, J.; Yin, J.; Fei, W.; Cao, Y.; Yu, J.; Yuan, L.; Gong, L.; Chen, J.; Deng, S.; Zhou, J.; Guo, W. Water-Evaporation-Induced-Electricity with Nanostructured Carbon Materials. *Nat. Nanotechnol.* **2017**, *12*, 317−321.
(40) Van der Heyden, F. H. J.; Stein, D.; Dekker, C. Streaming Currents in a Single Nanofluidic Channel. *Phys. Rev. Lett.* **2005**, *95*, 116104.
(41) Sun, J.; Li, P.; Qu, J.; Lu, X.; Xie, Y.; Gao, F.; Li, Y.; Gang, M.; Feng, Q.; Liang, H.; Xia, X.; Li, C.; Xu, S.; Bian, J. Electricity Generation From a Ni-Al Layered Double Hydroxide-Based Flexible Generator Driven by Natural Water Evaporation. *Nano Energy* **2019**, *57*, 269−278.
(42) Zhao, Y.; Hu, H.; Yang, X.; Yan, D.; Dai, Q. Tunable Electronic Transport Properties of 2D Layered Double Hydroxide Crystalline Microsheets with Varied Chemical Compositions. *Small* **2016**, *12*, 4471−4476.

https://doi.org/10.1021/acsomega.1c02398
ACS Omega 2021, 6, 20379−20387